APPLIED PHYSICS

Dynamic fracture of tantalum under extreme tensile stress

Bruno Albertazzi,[1,2]* Norimasa Ozaki,[1,3]* Vasily Zhakhovsky,[4,8]* Anatoly Faenov,[3,5] Hideaki Habara,[1,3] Marion Harmand,[6] Nicholas Hartley,[1,7] Denis Ilnitsky,[4,8] Nail Inogamov,[4,8] Yuichi Inubushi,[9,10] Tetsuya Ishikawa,[10] Tetsuo Katayama,[9,10] Takahisa Koyama,[9] Michel Koenig,[2,5] Andrew Krygier,[6] Takeshi Matsuoka,[5] Satoshi Matsuyama,[1] Emma McBride,[11,12] Kirill Petrovich Migdal,[4] Guillaume Morard,[6] Haruhiko Ohashi,[9] Takuo Okuchi,[13] Tatiana Pikuz,[3,5] Narangoo Purevjav,[13] Osami Sakata,[14] Yasuhisa Sano,[1] Tomoko Sato,[15] Toshimori Sekine,[15,16] Yusuke Seto,[17] Kenjiro Takahashi,[3] Kazuo Tanaka,[1,3] Yoshinori Tange,[9,18] Tadashi Togashi,[9,10] Kensuke Tono,[9,10] Yuhei Umeda,[15] Tommaso Vinci,[2] Makina Yabashi,[10] Toshinori Yabuuchi,[1,10] Kazuto Yamauchi,[1] Hirokatsu Yumoto,[9] Ryosuke Kodama[1,5,19]

The understanding of fracture phenomena of a material at extremely high strain rates is a key issue for a wide variety of scientific research ranging from applied science and technological developments to fundamental science such as laser-matter interaction and geology. Despite its interest, its study relies on a fine multiscale description, in between the atomic scale and macroscopic processes, so far only achievable by large-scale atomic simulations. Direct ultrafast real-time monitoring of dynamic fracture (spallation) at the atomic lattice scale with picosecond time resolution was beyond the reach of experimental techniques. We show that the coupling between a high-power optical laser pump pulse and a femtosecond x-ray probe pulse generated by an x-ray free electron laser allows detection of the lattice dynamics in a tantalum foil at an ultrahigh strain rate of $\dot{\varepsilon} \sim 2 \times 10^8$ to 3.5×10^8 s^{-1}. A maximal density drop of 8 to 10%, associated with the onset of spallation at a spall strength of ~17 GPa, was directly measured using x-ray diffraction. The experimental results of density evolution agree well with large-scale atomistic simulations of shock wave propagation and fracture of the sample. Our experimental technique opens a new pathway to the investigation of ultrahigh strain-rate phenomena in materials at the atomic scale, including high-speed crack dynamics and stress-induced solid-solid phase transitions.

INTRODUCTION

Dynamic high-pressure physics has gained increasing interest during the last decades in various domains such as planetology, including high-pressure phase diagram studies (*1*), crater impacts (*2*, *3*), and hypervelocity impacts from micrometeoroids and orbital debris (*4*, *5*), as well as technological and advanced material applications (*6*–*9*) such as laser shock peening (*10*), development of new materials (*11*), or adhesion tests (*12*). An important phenomenon for these studies is the dynamic fracture of a material under high-speed loading, which is critical for understanding its fundamental mechanical properties under shock loading. Dynamic fracture is characterized by the ejection of one or multiple fragments because of tensile stresses. The failure process under dynamic compression is due to the crossing of two release waves: In the case of a shocked material plate, one of these rarefaction waves is generated by unloading, starting from the front face of the plate, whereas the second one returns from the rear free surface after the reflection of the shock on it (*13*, *14*). Several experimental techniques have been developed to study the effect of dynamic damage (spallation) on materials at different strain rates and temperatures using macroscopic information, such as the evolution of free surface velocity and/or postmortem examination of the sample (*15*–*17*). However, no direct ultrafast observation of the stretching of the lattice at extreme deformation rates has been performed to date. More specifically, the high-pressure fracture properties of metals (such as Ta) or metal alloys are important for many applications, including for micrometeoroid and orbital debris shielding for future spacecraft and new generations of satellites, for plasma-facing components in nuclear power plants (*18*) and even for laser peening and adherence tests in a range of industrial applications. Previous experimental works (*19*–*22*) have all been restricted to indirect, macroscopic observations of the spallation process. Molecular dynamics (MD) simulations performed at strain rates of $\dot{\varepsilon} > 10^8$ s^{-1} (*23*) predict that the spall strength of Ta should be extremely high (>10 GPa), a pressure that could be calculated from an x-ray diffraction (XRD) signal.

Here, we report experimental results taking advantage of coupling a femtosecond x-ray free electron laser (XFEL) and a high-power optical laser beam to investigate, at the lattice level, the spallation (dynamic fracture) of a 5-μm polycrystalline Ta sample at extreme deformation rates, $\dot{\varepsilon} \sim 2 \times 10^8$ to 3.5×10^8 s^{-1}, and spall strength of 16.8 GPa. These results are then directly compared to large-scale MD simulations.

More generally, the study presented here shows an experimental technique, allowing for observation, at the lattice level, of the stretching

[1]Graduate School of Engineering, Osaka University, Suita, Osaka 565-0871, Japan. [2]LULI, École Polytechnique, CNRS, Commissariat à l'Energie Atomique et aux Energies Alternatives, Pierre and Marie Curie University (UPMC), 91128 Palaiseau, France. [3]Photon Pioneers Center, Osaka University, Suita, Osaka 565-0871, Japan. [4]Dukhov Research Institute of Automatics, ROSATOM, Moscow 127055, Russia. [5]Institute for Academic Initiatives, Osaka University, Suita, Osaka 565-0871, Japan. [6]Institut de Minéralogie, de Physique des Matériaux, et de Cosmochimie, Sorbonne Universités - UPMC, UMR CNRS 7590, Muséum National d'Histoire Naturelle, IRD UMR 206, F-75005 Paris, France. [7]Helmholtz-Zentrum Dresden-Rossendorf, Bautzner Landstrasse 400, 01328 Dresden, Germany. [8]L.D. Landau Institute for Theoretical Physics, Russian Academy of Science, Chernogolovka 142432, Russia. [9]Japan Synchrotron Radiation Research Institute, Sayo, Hyogo 679-5198, Japan. [10]RIKEN Center, Sayo, Hyogo 679-5148, Japan. [11]SLAC National Accelerator Laboratory, Menlo Park, CA 94025, USA. [12]European XFEL GmbH, Holzkoppel 4, D-22869 Schenefeld, Germany. [13]Institute for Planetary Materials, Okayama University, Misasa, Tottori 682-0193, Japan. [14]Synchrotron X-ray Station at Spring-8, National Institute for Materials Science (NIMS), Sayo, Hyogo 679-5148, Japan. [15]Graduate School of Science, Hiroshima University, Higashihiroshima 739-8526, Japan. [16]Center for High Pressure Science and Technology Advanced Research, Pudong, Shanghai 201203, China. [17]Graduate School of Science, Kobe University, Kobe 657-8501, Japan. [18]Geodynamics Research Center, Ehime University, Matsuyama, Ehime 790-8577, Japan. [19]Institute of Laser Engineering, Osaka University, 2-6 Yamada-oka, Suita, Osaka 565-0871, Japan. *Corresponding author. Email: bruno.albertazzi@polytechnique.edu (B.A.); norimasa.ozaki@eie.eng.osaka-u.ac.jp (N.O.); vasily@mpd3.com (V.Z.)

of a material under extreme deformation rates and determination of one of its universal properties: the spall strength. At this scale, it is then possible to directly compare the experimental results with MD simulation to develop and/or further constrain interatomic potential for a given material. This method has strong implications for material characterization and optimization, investigation of material properties under high impact, or the development of new materials as it bridges the gap in the understanding of the relationship between atomic structure and material properties.

RESULTS AND DISCUSSION

The pump-probe experiment was performed at the SPring-8 Angstrom Compact Free Electron Laser (SACLA), Japan (*24*, *25*). The experimental setup is shown in Fig. 1. An optical laser at 800-nm wavelength, with a pulse duration of ~660-ps full width at half maximum (FWHM) and an energy on target up to 1 J, was focused down to ~280-μm FWHM, resulting in an on-target intensity of ~2.5×10^{12} W/cm^2, to generate a shock wave in a 5-μm-thick polycrystalline Ta target. At the rear side of the target with respect to the pump laser, a 7-fs quasi-monochromatic XFEL pulse, with ~10-keV photon energy (energy bandwidth of ~0.5%) and ~10^{11} photons per pulse, was used to probe the crystallographic lattice spacing d of the sample. The target was placed at a 20° incident angle compared to the XFEL beam axis, which was focused in one direction down to ~17 μm using a mirror, whereas the other axis was adjusted to ~200 μm by a two-quadrant slit. X-rays were then diffracted by the orderly array of the body-centered cubic (bcc) (002) Ta planes into a Debye-Scherrer diffraction ring. A part of the diffraction ring was observed on a one-megapixel array detector (*26*) to determine the lattice spacing d of the sample (see Fig. 1A). In that way, a higher 2θ angle would correspond to a compression, whereas a lower 2θ angle refers to an expansion of the lattice (see the Supplementary Materials). Note that our experimental configuration allows us to study the lattice deformation and fracture of the Ta sample in a region corresponding to the submicrometer penetration depth of the 10-keV x-rays inside the material (L ~ 0.85 μm). This short penetration depth means that our data are only sensitive to a small portion of the sample, rather than integrating over the whole thickness of the sample as in a transmissive configuration (*27*), and are therefore extremely sensitive to the atomic motion very near the sample free surface. In addition, this configuration separates the probed region from the laser-matter interaction occurring at the front surface of the target, allowing us to probe a region in the target where the shock wave is well established.

The evolution of lattice deformation associated with the ultrafast fracture in Ta is given by a time series of XRD patterns taken by varying the delay between the pump and the probe beam, where $t = 0$ is defined at the beginning of the laser pulse (see the Supplementary Materials). The mean crystallite dimension (τ) of our sample is on the order of ~20 nm, related to the broadening of the measured peak at zero pressure and room temperature (see Fig. 1B) by the Scherrer equation.

The 2θ angle of the unstrained bcc (002) lattice plane of our Ta sample measured in the experiment is 43.76° (see Fig. 2) corresponding to a spacing d = 1.652 Å and density of ~16.66 g/cm^3. Within the first 50 ps presented in Fig. 2 (t = 1475 and 1525 ps), one can observe two or more peaks related to a compression and an expansion (stretching) of the lattice in a part of the x-ray probed zone (see Fig. 2A). The observed compression (2θ > 43.76°) at these early times corresponds to the shocked compressed part of the sample. The simultaneous expansion (2θ < 43.76°) is associated with the propagation of the rarefaction wave in the compressed sample that was produced when the shock wave

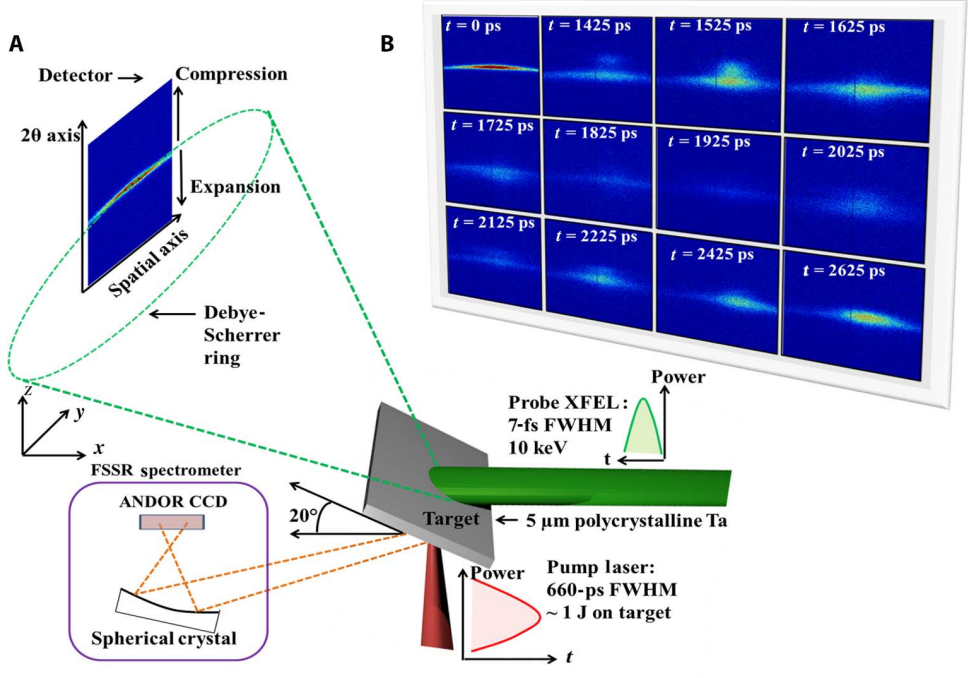

Fig. 1. The pump-probe experiment at SACLA. (**A**) Experimental configuration, where a 5-μm-thick polycrystalline Ta sample is compressed by a pump (optical) laser and the diffraction is observed preferentially in the bcc <001> direction. An ultrafast (7 fs) x-ray beam focused in the z direction probes the lattice arrangement of the sample and generates a Debye-Scherrer ring. (**B**) A part of the Debye-Scherrer ring is recorded by the multiport charge-coupled device (MPCCD) detector for the bcc (002) plane of Ta at different times during the interaction. All the experimental images have the same color scale.

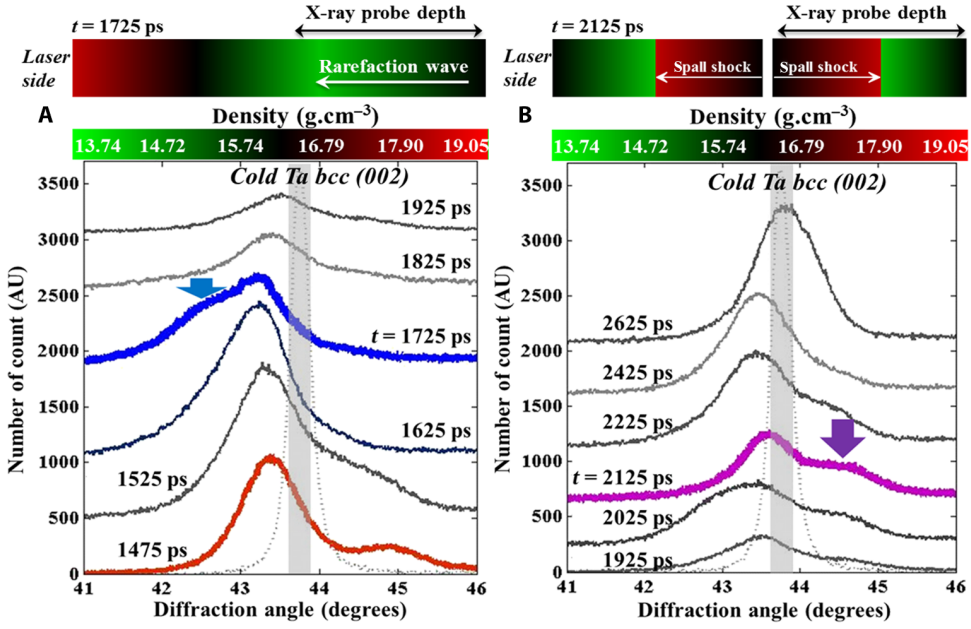

Fig. 2. Experimental profiles of the stretching and postspallation compression in the Ta sample. (**A**) Observation of the stretching in the experiment of the (002) plane of Ta using an azimuthal integration of the diffraction signal obtained onto the MPCCD detector (blue arrow). (**B**) Observation of the compression wave (purple arrow) due to the relaxation of the tension after spallation in the experiment of the (002) plane of Ta using an azimuthal integration of the diffraction signal obtained onto the MPCCD detector. The onset at the top left corresponds to the maximum stretching of the sample reached at a time $t = 1725$ ps after the beginning of the interaction, whereas the onset at the top right corresponds to the dynamic fracture of the sample responsible for the generation of a compression wave propagating in the spall layer. The laser comes from the left, and the XFEL probe comes from the right. These illustrations are not to scale.

reached the free surface. These two phenomena of compression and expansion are contained in a very small space (that is, the region of the penetration depth of the x-rays) and time, which also demonstrates that a very sharp discrete rarefaction wavefront is created, propagating at ~4.5 km/s.

At later times (for example, $t = 1625$ ps), no lattices are compressed and one can only observe a peak from stretched lattices. The maximum expansion, which is related to the ultrafast fracture of the sample, occurs at $t = 1725$ ps, where a second peak appears at $2\theta \sim 42.42°$. The two positions of the maximum of the major peaks retrieved at that time have a spacing $d = 1.679$ and 1.709 Å, which correspond to densities of $\rho = 15.87$ and 15.04 g/cm^3, respectively. Those densities correspond to the stretched solid states with respective pressures of −8.7 and −16.78 GPa according to the Birch-Murnagham equation of state (see the Supplementary Materials) (*28*–*30*). The later times, that is, $t \geq 1925$ ps, unambiguously show the progressive emergence of a compression wave (see Fig. 2B) with the appearance of a peak at $2\theta \sim 44.60°$. This compression wave, referred to as the "spall shock" in the following, is generated by ultrafast void nucleations and propagates from the void locations toward the free surface of the spalled layer. The sudden stress relaxation from the negative to ambient pressure in the stretched lattice zone gives rise to the emergence of a strong recompression wave, which propagates in the spalled layer of the material. As a consequence, this spall shock is a strong signature of an initiation of the ultrafast fracture of the sample. The maximum compression due to the spall shock is observed at $t = 2125$ ps, where the amplitude of the peak at $2\theta \sim 44.60°$ is maximized. Finally, at the latest probing time ($t = 2625$ ps), the peak is almost at the initial position, although it is wider, probably due to a distribution of different strain (positive or negative) and residual temperature effects.

The experimental data allow us to directly determine the strain rate $\dot{\varepsilon} = \partial\varepsilon/\partial t$, where $\varepsilon = (d(t) - d_0)/d_0$, with $d(t)$ corresponding, in our case, to the spacing d, assuming a uniaxial deformation of the sample, and d_0 to the initial d spacing. Before spallation (that is, $t = 1725$ ps), the averaged elongation of the material is $d(t = 1725\ \text{ps}) = 1.7094$ Å and $d_0(t = 1625\ \text{ps}) = 1.679$ Å. The temporal dynamics shown in Fig. 2A inform us that the elongation from d_0 to $d(t)$ takes place within 100 ps. Therefore, it is only possible to give a lower limit of the experimental strain rate using this method, which should be $\dot{\varepsilon} > 1.81 \times 10^8\ \text{s}^{-1}$.

A large-scale MD simulation of a single-crystal Ta film was performed to directly compare and interpret the experimental results (see the Supplementary Materials for more details). A movie of the MD simulation is presented in the Supplementary Materials. At early time points, the MD simulation shows the propagation of the rarefaction wave from the free rear-side surface back into the sample, implying the emergence of tension and a lower density than the initial one. A direct comparison of diffracted x-ray signals coming from the MD simulation and experimental data is displayed in Fig. 3 (A and B). The overall trend (compare Fig. 3B) is well reproduced by the MD simulation, where the time evolution of the diffraction angle during expansion of the lattice and the propagation of the spall shock are in agreement. Therefore, the physical mechanism of the dynamic fracture of the sample is given by the MD simulation.

The dynamic fracture of the sample starts at $t = 1800$ ps. The spall strength then corresponds to the tension (negative pressure) present just before the spallation occurs, that is, ~−18 GPa (see the Supplementary Materials). This stress in the rarefaction wave is reached after $t = 1800$ ps in a wide fracture zone with length of about 1700 nm, where many nanovoids start to nucleate independently, as can be seen in Fig. 3C.

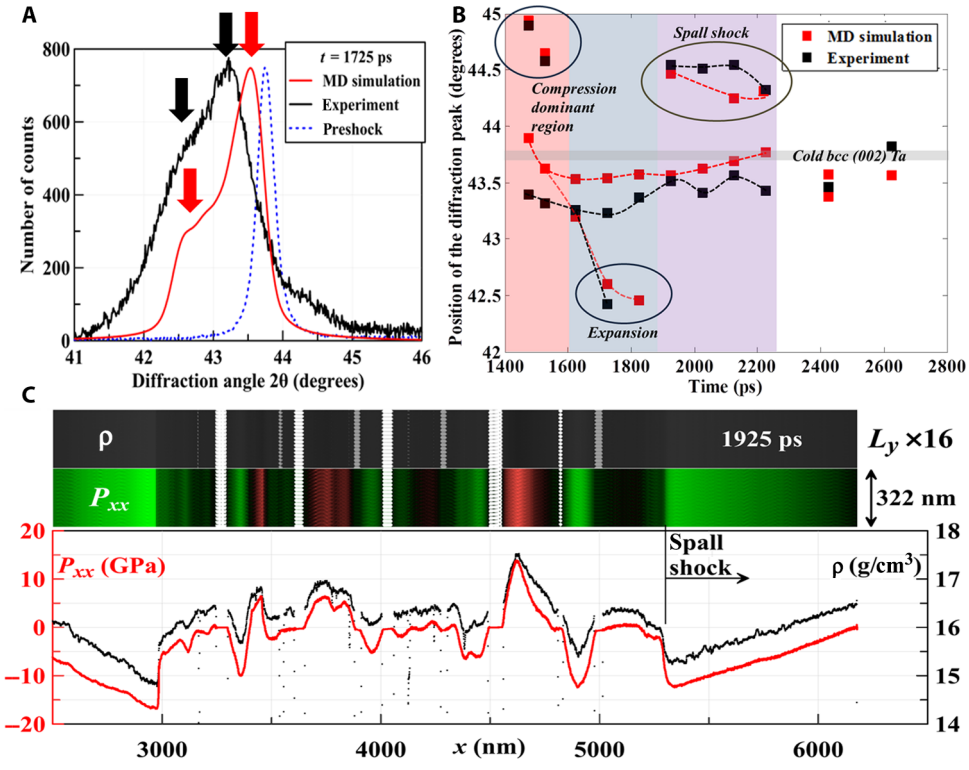

Fig. 3. MD simulation and direct comparison with experimental data. (**A**) Comparison of the diffraction signal obtained from the experiment and simulated by the MD just before spallation, where the stretching of the lattice is the most important at 1725 ps after the beginning of the interaction. The black and red arrows indicate the position of the maximum of the diffraction peaks. (**B**) Direct comparison between the position of the maximum of the different diffraction peaks in the experiment and in the simulation (t = 0 being defined in the same manner in both cases). (**C**) Two-dimensional (2D) maps shown in the middle panel corresponding to the spatial distribution of density ρ(x,y) and the longitudinal component of the pressure tensor ($P_{xx} \equiv -\sigma_{xx}$) are built by cloning the simulated narrow sample with L_y = 20 nm by a factor of 16. White gaps correspond to pores or voids. For the P_{xx} map, the green color represents negative pressure and the red color represents positive pressure. The corresponding profiles of density and pressure P_{xx} at a time of 1925 ps after the beginning of the interaction are displayed in the bottom panel.

Because the voids appear with a time spread of ~10 ps and each new void relaxes the surrounding tensile stress, only one void per about 150 nm can survive and grow further. Because of the periodical boundary condition imposed along y and z axes, the growth of voids is limited by the size of the MD simulation ($L_{y,z}$ = 20 nm). Some of them lead to multiple fractures of the sample, whereas others, which stop increasing in size while still smaller than 20 nm, are just closed pores (illustrated in gray color in Fig. 3C). The ultrafast fracture of the sample generates a shock wave (spall shock) starting from the location of the voids, which propagates through the spalled layer (which starts at x ~ 5000 nm in Fig. 3C). The spall shock pressure and density profile exhibit almost a "plateau" of ~200 nm with an amplitude of ~10 GPa (~17.2 g/cm^3; see fig. S3B). Some material at the front of the shock wave still remains at a negative pressure (≤−1 GPa) because of tensile stresses. The spall shock compresses the sample up to a maximum density of ~17.5 g/cm^3, which corresponds to a pressure of ~15 GPa (see the Supplementary Materials).

The strain rate is determined from the mass velocity profile $u(x)$ obtained from the MD simulation (see the Supplementary Materials) and gives $\dot{\varepsilon} = 3.5 \times 10^8\ s^{-1}$ just before the first rightmost spallation, that is, at a time of t = 1788 ps after the beginning of the interaction. It is consistent with the lower limit calculated using the experimental data $\dot{\varepsilon} > 1.81 \times 10^8\ s^{-1}$, and it is also possible to obtain a "pseudo-experimental strain rate" using (i) the elongation of the sample given by the experimental data and (ii) the time t of the fracture observed in the MD simulation. In that case, the pseudo-experimental strain rate is $\dot{\varepsilon} \sim 2.9 \times 10^8\ s^{-1}$, again in excellent agreement with the MD simulation.

In conclusion, we have demonstrated the feasibility of recording the evolution of material at extreme deformation rates $\dot{\varepsilon}$ ~2×10^8 to $3.5 \times 10^8\ s^{-1}$ using a real-time x-ray monitoring technique, opening the way to investigating the dynamic fracture of materials at the lattice level and revealing the atomic structure under tension. Using this technique, a maximal density decrease of 8 to 10%, associated with the onset of spallation in a tantalum sample, was directly measured. Thus, a spall strength of ~16.8 GPa was calculated. This direct method should provide a more accurate spall strength than one estimated from the measured pullback velocity of the rear-side boundary of the spalled layer (*31*), allow the study of dynamical fracture (spallation) of a material at ultrahigh strain rate and atomic scale, and provide a way to accurately benchmark MD simulation. This is a crucial point for future technological and advanced material creation.

The experimental data show extremely good agreement with both previous results and our MD simulation (see the Supplementary Materials), which not only paves the way toward the direct measurement of spall strength of materials as a function of strain rate but also highlights the usefulness of these facilities to investigation of high-speed crack dynamics and uncommon stress-induced solid-solid phase transitions (*32*). These transitions could have a significant impact in the industry to develop new materials, allowing interesting mechanical

properties for the development of spacecraft, satellite, and plasma-facing components in nuclear power plant facilities.

MATERIALS AND METHODS

The experiment was carried out on the beamline 3 (BL3) at SACLA. The spectrum of the x-ray beam was recorded on-shot to minimize uncertainties related to the evaluation of the crystallographic lattice spacing d of the sample. The optical laser beam was focused on the target using a $f = 500$ lens. The next step was to defocus it to have a focal spot larger than the one of the x-ray beam. The synchronization of the main optical beam with the XFEL beam was performed using the following procedure: Initially, we measured the time difference between the optical laser and XFEL beams with a photodiode from a polyimide sample at the target center chamber. To have a precision of ~25 ps for the beginning of pulse, we used a specially designed target made of a 500-nm-thick polycrystalline Au foil coating deposited on a 100-μm-thick acrylic substrate. The optical beam irradiated the Au side of the target, and the XFEL beam probed the spacing d (in measuring the 2θ angle) through the acrylic [for more details, see Hartley *et al.* (*33*)]. The delay between the optical and the XFEL was then changed to observe when the Au lines became broadened for the first time due to sample heating. In that case, we could evaluate a typical laser intensity that corresponded to our time $t = 0$ (see the Supplementary Materials).

SUPPLEMENTARY MATERIALS

Supplementary material for this article is available at http://advances.sciencemag.org/cgi/content/full/3/6/e1602705/DC1

fig. S1. Single-shot x-ray spectra of Ta plasma irradiated by the high-power optical laser.
fig. S2. Pulse shape of the optical beam at target center chamber.
fig. S3. Velocity of the Lagrangian particle provided by hydrodynamic (MULTI) modeling.
fig. S4. Comparison between the new EAM Ta potential and experimental shock Hugoniot curve.
fig. S5. Shadowgraph of mass distribution after nucleation of first voids in the MD-simulated Ta sample.
fig. S6. MD simulation of the experiment.
fig. S7. Determination of the strain rate from the flow velocity profile just before nucleation of the first voids in the MD simulation.
fig. S8. Determination of the strain rate from the flow velocity profile just before nucleation of the first voids in the MD simulation.
fig. S9. Direct comparison between experimental profiles and x-ray profiles derived from the MD simulation.
fig. S10. Experimental determination of the position of the different peaks at $t = 1725$ ps using the Gaussian method.
fig. S11. Experimental determination of the position of the different peaks at $t = 2125$ ps using the Gaussian method.
fig. S12. Experimental determination of the position of the different peaks at $t = 2125$ ps using the Lorentzian method.
fig. S13. Spall strength versus strain rate for tantalum.
table S1. Pressure and density retrieved from the experimental results at $t = 1725$ ps displayed in fig. S10.
table S2. Pressure and density retrieved from the experimental results at $t = 2125$ ps displayed in fig. S11.
movie S1. Evolution of density and pressure in the sample given by MD simulation.
movie S2. Experimental data obtained at SACLA.
References (*34*–*51*)

REFERENCES AND NOTES

1. C. S. Yoo, J. Akella, A. J. Campbell, K. H. Mao, R. J. Hemley, Phase diagram of iron by in situ x-ray diffraction: Implications for Earth's core. *Science* **270**, 1473–1475 (1995).
2. K. Ernstson, M. R. Rampino, M. Hiltl, Cratered cobbles in Triassic Buntsandstein conglomerates in northeastern Spain: An indicator of shock deformation in the vicinity of large impacts. *Geology* **29**, 11–14 (2001).
3. H. J. Melosh, Impact ejection, spallation, and the origin of meteorites. *Icarus* **59**, 234–260 (1984).
4. www.nasa.gov/centers/wstf/laboratories/hypervelocity/mmod.html
5. S. Ryan, E. L. Christiansen, Hypervelocity impact testing of advanced materials and structures for micrometeoroid and orbital debris shielding. *Acta Astronaut.* **83**, 216–231 (2013).
6. P. F. McMillan, New materials from high-pressure experiments. *Nat. Mater.* **1**, 19–25 (2002).
7. M. Boustie, F. Cottet, Experimental and numerical study of laser induced spallation into aluminium and copper targets. *J. Appl. Phys.* **69**, 7533 (1991).
8. V. V. Brazhkin, High-pressure synthesized materials: Treasures and hints. *High Pressure Res.* **27**, 333–351 (2007).
9. V. L. Solozhenko, O. O. Kurakevych, Y. Le Godec, Creation of nanostructures by extreme conditions: High-pressure synthesis of ultrahard nanocrystalline cubic boron nitride. *Adv. Mater.* **24**, 1540–1544 (2012).
10. Y. Cao, Y. C. Shin, Shock wave propagation and spallation study in laser shock peening. *J. Eng. Mater. Technol.* **132**, 041005 (2010).
11. R. Ecault, M. Boustie, F. Touchard, F. Pons, L. Berthe, L. Chocinski-Arnault, B. Ehrhart, C. Bockenheimer, A study of composite material damage induced by laser shock waves. *Compos. Part A Appl. Sci. Manuf.* **53**, 54–64 (2013).
12. C. Bolis, L. Berthe, M. Boustie, M. Arrigoni, S. Barradas, M. Jeandin, Physical approach to adhesion testing using laser-driven shock waves. *J. Phys. D Appl. Phys.* **40**, 3155–3163 (2007).
13. T. Antoun, L. Seaman, D. R. Curran, G. I. Kanel, S. V. Razorenov, A. V. Utkin, *Spall Fracture* (Springer, 2002).
14. G. I. Kanel, Spall fracture: Methodological aspects, mechanisms and governing factors. *Int. J. Fract.* **163**, 173–191 (2010).
15. T. de Rességuier, M. Hallouin, Effects of the α-ε phase transition on wave propagation and spallation in laser shock-loaded iron. *Phys. Rev. B* **77**, 174107 (2008).
16. J. R. Asay, T. Ao, T. J. Vogler, J.-P. Davis, G. T. Gray III, Yield strength of tantalum for shockless compression to 18 GPa. *J. Appl. Phys.* **106**, 073515 (2009).
17. L. Soulard, J. Bontaz-Carion, J. P. Cuq-Lelandais, Experimental and numerical study of the tantalum single crystal spallation. *Eur. Phys. J. B.* **85**, 332 (2012).
18. R. A. Pitt, S. Carpentier, F. Escourbiac, T. Hirai, V. Komarov, S. Lisgo, A. Kukushkin, A. Loarte, M. Merola, A. Sashala Naik, R. Mitteau, M. Sugihara, B. Bazylev, P. C. Stangeby, A full tungsten divertor for ITER: Physics issues and design status. *J. Nucl. Mater.* **438**, S48–S56 (2013).
19. G. Roy, Vers une modélisation approfondie de l'endommagement ductile dynamique. Investigation expérimentale d'une nuance de tantale et développements théoriques, thesis, Université de Poitiers (2003).
20. L. Soulard, J. P. CuqLelandais, M. Boustie, *Experimental and Molecular Dynamics Study of Spallation in Tantalum Single Crystal* (Khariton's Topical Scientific Readings, 2009).
21. S. I. Abrosimov, P. S. Komarov, A. V. Ovchinnikov, E. V. Struleva, M. B. Agranat, Deformation dynamics and spallation strength of aluminium under a single-pulse action of a femtosecond laser. *Quantum Electron.* **43**, 242–245 (2013).
22. S. I. Ashitkov, P. S. Komarov, E. V. Struleva, M. B. Agranat, G. I. Kanel, K. V. Khishchenko, The behavior of tantalum under ultrashort loads induced by femtosecond laser. *J. Phys. Conf. Ser.* **653**, 012001 (2015).
23. S.-N. Luo, Shock compression and spallation of single crystal tantalum. *AIP Conf. Proc.* **1426**, 1259–1262 (2012).
24. T. Ishikawa, H. Aoyagi, T. Asaka, Y. Asano, N. Azumi, T. Bizen, H. Ego, K. Fukami, T. Fukui, Y. Furukawa, S. Goto, H. Hanaki, T. Hara, T. Hasegawa, T. Hatsui, A. Higashiya, T. Hirono, N. Hosoda, M. Ishii, T. Inagaki, Y. Inubushi, T. Itoga, Y. Joti, M. Kago, T. Kameshima, H. Kimura, Y. Kirihara, A. Kiyomichi, T. Kobayashi, C. Kondo, T. Kudo, H. Maesaka, X. M. Maréchal, T. Masuda, S. Matsubara, T. Matsumoto, T. Matsushita, S. Matsui, M. Nagasono, N. Nariyama, H. Ohashi, T. Ohata, T. Ohshima, S. Ono, Y. Otake, C. Saji, T. Sakurai, T. Sato, K. Sawada, T. Seike, K. Shirasawa, T. Sugimoto, S. Suzuki, S. Takahashi, H. Takebe, K. Takeshita, K. Tamasaku, H. Tanaka, R. Tanaka, T. Tanaka, T. Togashi, K. Togawa, A. Tokuhisa, H. Tomizawa, K. Tono, S. Wu, M. Yabashi, M. Yamaga, A. Yamashita, K. Yanagida, C. Zhang, T. Shintake, H. Kitamura, N. Kumagai, A compact X-ray free-electron laser emitting in the sub-ångström region. *Nat. Photonics* **6**, 540–544 (2012).
25. K. Tono, T. Togashi, Y. Inubushi, T. Sato, T. Katayama, K. Ogawa, H. Ohashi, H. Kimura, S. Takahashi, K. Takeshita, H. Tomizawa, S. Goto, T. Ishikawa, M. Yabashi, Beamline, experimental stations and photon beam diagnostics for the hard x-ray free electron laser of SACLA. *New J. Phys.* **15**, 083035 (2013).
26. T. Kameshima, S. Ono, T. Kudo, K. Ozaki, Y. Kirihara, K. Kobayashi, Y. Inubushi, M. Yabashi, T. Horigome, A. Holland, K. Holland, D. Burt, H. Murao, T. Hatsui, Development of an X-ray pixel detector with multi-port charge-coupled device for X-ray free-electron laser experiments. *Rev. Sci. Instrum.* **85**, 033110 (2014).
27. D. Milathianaki, S. Boutet, G. J. Williams, A. Higginbotham, D. Ratner, A. E. Gleason, M. Messerschmidt, M. M. Seibert, D. C. Swift, P. Hering, J. Robinson, W. E. White, J. S. Wark, Femtosecond visualization of lattice dynamics in shock-compressed matter. *Science* **342**, 220–223 (2013).
28. F. Birch, Finite elastic strain of cubic crystals. *Phys. Rev.* **71**, 809–824 (1947).

29. F. D. Murnagham, Finite deformations of an elastic solid. *Am. J. Math.* **49**, 235–260 (1937).
30. F. D. Murnagham, The compressibility of media under extreme pressures. *Proc. Natl. Acad. Sci. U.S.A.* **30**, 244–247 (1944).
31. S. Eliezer, E. Moshe, D. Eliezer, Laser-induced tension to measure the ultimate trength of metals related to the equation of state. *Laser Part. Beams* **20**, 87–92 (2002).
32. Z. G. Nicolaou, A. E. Motter, Mechanical metamaterials with negative compressibility transitions. *Nat. Mater.* **11**, 608–613 (2012).
33. N. J. Hartley, N. Ozaki, T. Matsuoka, B. Albertazzi, A. Faenov, Y. Fujimoto, H. Habara, M. Harmand, Y. Inubushi, T. Katayama, M. Koenig, A. Krygier, P. Mabey, Y. Matsumura, S. Matsuyama, E. E. McBride, K. Miyanishi, G. Morard, T. Okuchi, T. Pikuz, O. Sakata, Y. Sano, T. Sato, T. Sekine, Y. Seto, K. Takahashi, K. A. Tanaka, Y. Tange, T. Togashi, Y. Umeda, T. Vinci, M. Yabashi, T. Yabuuchi, K. Yamauchi, R. Kodama, Ultrafast observation of lattice dynamics in laser-irradiated gold foils. *Appl. Phys. Lett.* **110**, 071905 (2017).
34. A. Y. Faenov, S. A. Pikuz, A. I. Erko, B. A. Bryunetkin, V. M. Dyakin, G. V. Ivanenkov, A. R. Mingaleev, T. A. Pikuz, V. M. Romanova, T. A. Shelkovenko, High-performance x-ray spectroscopic devices for plasma microsources investigations. *Phys. Scr.* **50**, 333–338 (1994).
35. T. A. Pikuz, A. Y. Faenov, N. Ozaki, N. J. Hartley, B. Albertazzi, T. Matsuoka, K. Takahashi, H. Habara, Y. Tange, S. Matsuyama, K. Yamauchi, R. Ochante, K. Sueda, O. Sakata, T. Sekine, T. Sato, Y. Umeda, Y. Inubushi, T. Yabuuchi, T. Togashi, T. Katayama, M. Yabashi, M. Harmand, G. Morard, M. Koenig, V. Zhakhovsky, N. Inogamov, A. S. Safronova, A. Stafford, I. Y. Skobelev, S. A. Pikuz, T. Okuchi, Y. Seto, K. A. Tanaka, T. Ishikawa, R. Kodama, Indirect monitoring shot-to-shot shock waves strength reproducibility during pump-probe experiments. *J. Appl. Phys.* **120**, 035901 (2016).
36. R. Ramis, R. Schmalz, J. Meyer-Ter-Vehn, MULTI—A computer code for one-dimensional multigroup radiation hydrodynamics. *Comput. Phys. Commun.* **49**, 475–505 (1988).
37. www.lanl.gov/org/padste/adtsc/theoretical/physics-chemistry-materials/sesame-database.php
38. V. V. Zhakovskii, N. A. Inogamov, Y. V. Petrov, S. I. Ashitkov, K. Nishihara, Molecular dynamics simulation of femtosecond ablation and spallation with different interatomic potentials. *Appl. Surf. Sci.* **255**, 9592–9596 (2009).
39. G. Kresse, J. Furthmüller, Efficient iterative schemes for ab initio total-energy calculations using a plane-wave basis set. *Phys. Rev. B* **54**, 11169–11186 (1996).
40. G. Kresse, D. Joubert, From ultrasoft pseudopotentials to the projector augmented-wave method. *Phys. Rev. B* **59**, 1758–1775 (1999).
41. P. E. Blöchl, Projector augmented-wave method. *Phys. Rev. B* **50**, 17953–17979 (1994).
42. J. P. Perdew, K. Burke, M. Ernzerhof, Generalized gradient approximation made simple. *Phys. Rev. Lett.* **77**, 3865–3868 (1996).
43. H. J. Monkhorst, J. D. Pack, Special points for Brillouin-zone integrations. *Phys. Rev. B* **13**, 5188–5192 (1976).
44. J. A. Nelder, R. Mead, A simplex method for function minimization. *Comput. J.* **7**, 308–313 (1965).
45. Shock wave database, http://teos.ficp.ac.ru/rusbank/
46. W. F. Gale, T. C. Totemeier, *Smithells Metals Reference Book* (Elsevier Butterworth-Heinemann, ed. 8, 2004), pp. 15–36.
47. J. H. Li, S. H. Liang, H. B. Guo, B. X. Liu, Four-parameter equation of state of solids. *Appl. Phys. Lett.* **87**, 194111 (2005).
48. H. Cynn, C.-S. Yoo, Equation of state of tantalum to 174 GPa. *Phys. Rev. B* **59**, 8526–8529 (1999).
49. J. P. Cuq-Lelandais, M. Boustie, L. Soulard, L. Berthe, T. De Rességuier, P. Combis, J. Bontaz-Carion, E. Lescoute, Study of spallation by sub-picosecond laser driven shocks in metals. *EPJ Web Conf.* **10**, 00014 (2010).
50. S. V. Razorenov, G. V. Garkushin, G. I. Kanel, O. N. Ignatova, The spall strength and Hugoniot elastic limit of tantalum with various grain size. *AIP Conf. Proc.* **1426**, 991 (2012).
51. S. A. Abrosimov, A. P. Bazhulin, V. V. Voronov, A. A. Geras'kin, I. K. Krasyuk, P. P. Pashinin, A. Y. Semenov, I. A. Stuchebryukhov, V. V. Khishchenko, V. Fortov, Specific features of the behavior of targets under negative pressures created by a picosecond laser pulse. *Quantum Electron.* **43**, 246–251 (2013).

Acknowledgments: We would like to thank Y. Kimura for her support with target fabrication. **Funding:** The XFEL experiment was performed at the BL3 of SACLA with the approval of the Japan Synchrotron Radiation Research Institute (proposal nos. 2014B8068, 2015A8023, and 2015A8066). This work was supported in part by Japan Society for the Promotion of Science (JSPS) KAKENHI (grant nos. 15K13609 and 15H05751), JSPS core-to-core program on International Alliance for Material Science in Extreme States with High Power Laser and XFEL, and the X-ray Free Electron Laser Priority Strategy Program at Osaka University from the Ministry of Education, Culture, Sports, Science, and Technology (contract 12005014). V.Z., N.I., D.I., and K.P.M. were supported by Russian Science Foundation grant 14-19-01599. M.H., G.M., and A.K were supported by the French Agence Nationale de la Recherche (ANR) with ANR IRONFEL 12-PDOC-0011. Y.T. received funding from JSPS KAKENHI (grant no. 25707041). E.M. acknowledges funding from the Volkswagen Foundation. **Author contributions:** B.A., N.O., T.I., O.S., and R.K. conceived the project. B.A., N.O., H.H., M.H., N.H., Y.I., T. Katayama, M.K., A.K., T.M., E.M., G.M., T.O., N.P., T. Sato, T. Sekine, Y. Seto, K. Takahashi, K. Tanaka, Y.T., T.T., K. Tono, Y.U., M.Y., and T.Y. performed the experiment. A.F. and T.P. monitored the stability of shock pressure with spectroscopy. T. Koyama, T.M., H.O., Y. Seto, K.Y., and H.Y. performed the 1D focusing of the XFEL beam. B.A. analyzed the experimental data and interpreted the experimental results with N.O and V.Z. K.P.M. performed density functional theory calculations. The EAM potential for Ta was developed by V.Z. MD simulations were performed by V.Z., D.I., and N.I. Hydrodynamic simulations were performed by T.V. The paper was written by B.A., N.O., and V.Z. All authors contributed to the work presented here and to the final paper. **Competing interests:** The authors declare that they have no competing interests. **Data and materials availability:** All data needed to evaluate the conclusions in the paper are present in the paper and/or the Supplementary Materials. Additional data related to this paper may be requested from the authors.

Submitted 2 November 2016
Accepted 10 April 2017
Published 2 June 2017
10.1126/sciadv.1602705

Citation: B. Albertazzi, N. Ozaki, V. Zhakhovsky, A. Faenov, H. Habara, M. Harmand, N. Hartley, D. Ilnitsky, N. Inogamov, Y. Inubushi, T. Ishikawa, T. Katayama, T. Koyama, M. Koenig, A. Krygier, T. Matsuoka, S. Matsuyama, E. McBride, K. P. Migdal, G. Morard, H. Ohashi, T. Okuchi, T. Pikuz, N. Purevjav, O. Sakata, Y. Sano, T. Sato, T. Sekine, Y. Seto, K. Takahashi, K. Tanaka, Y. Tange, T. Togashi, K. Tono, Y. Umeda, T. Vinci, M. Yabashi, T. Yabuuchi, K. Yamauchi, H. Yumoto, R. Kodama, Dynamic fracture of tantalum under extreme tensile stress. *Sci. Adv.* **3**, e1602705 (2017).

Science Advances

Dynamic fracture of tantalum under extreme tensile stress

Bruno Albertazzi, Norimasa Ozaki, Vasily Zhakhovsky, Anatoly Faenov, Hideaki Habara, Marion Harmand, Nicholas Hartley, Denis Ilnitsky, Nail Inogamov, Yuichi Inubushi, Tetsuya Ishikawa, Tetsuo Katayama, Takahisa Koyama, Michel Koenig, Andrew Krygier, Takeshi Matsuoka, Satoshi Matsuyama, Emma McBride, Kirill Petrovich Migdal, Guillaume Morard, Haruhiko Ohashi, Takuo Okuchi, Tatiana Pikuz, Narangoo Purevjav, Osami Sakata, Yasuhisa Sano, Tomoko Sato, Toshimori Sekine, Yusuke Seto, Kenjiro Takahashi, Kazuo Tanaka, Yoshinori Tange, Tadashi Togashi, Kensuke Tono, Yuhei Umeda, Tommaso Vinci, Makina Yabashi, Toshinori Yabuuchi, Kazuto Yamauchi, Hirokatsu Yumoto and Ryosuke Kodama

Sci Adv **3** (6), e1602705.
DOI: 10.1126/sciadv.1602705